Modeling and Characterization of High-Efficiency Silicon Solar Cells Fabricated by Rapid Thermal Processing, Screen Printing, and Plasma-Enhanced Chemical Vapor Deposition

Parag Doshi, Jose Mejia, Keith Tate, and Ajeet Rohatgi, *Fellow, IEEE*

***Abstract*—This paper presents, for the first time, the successful integration of three rapid, low-cost, high-throughput technologies for silicon solar cell fabrication, namely: rapid thermal processing (RTP) for simultaneous diffusion of a phosphorus emitter and aluminum back surface field; screen printing (SP) for the front grid contact; and low-temperature plasma-enhanced chemical vapor deposition (PECVD) of SiN for antireflection coating and surface passivation. This combination has resulted in 4 cm^2 cells with efficiencies of 16.3% and 15.9% on 2 Ω-cm FZ and Cz, respectively, as well as 15.4% efficient, 25-cm^2 FZ cells. Despite the respectable RTP/SP/PECVD efficiencies, cells formed by conventional furnace processing and photolithography (CFP/PL) give ∼2% (absolute) greater efficiencies. Through in-depth modeling and characterization, this efficiency difference is quantified on the basis of emitter design and front surface passivation, grid shading, and quality of contacts. Detailed analysis reveals that the difference is primarily due to the requirements of screen printing and not RTP.**

I. Introduction and Background

COST-EFFECTIVENESS is the major obstacle facing the silicon solar cell industry. This paper presents the development and integration of cell process techniques that are suitable for industrial production and have the potential of becoming the lowest-cost and highest throughput process for the fabrication of silicon photovoltaic devices with high energy conversion efficiency. We present the fundamental understanding and engineering of the rapid thermal processing/screen printing/plasma enhanced chemical vapor deposition (RTP/SP/PECVD) process, which not only simplifies processing, but also produces 15.5%–16% efficient, manufacturable cells on single-crystal silicon. Unlike other high-efficiency screen-printed cell designs [made by conventional furnace processing (CFP)] reported in the literature [1]–[4], these RTP/SP/PECVD cells involve neither oxide passivation nor fine-line printing ($\leq$60 μm grid fingers), selective emitter, or texturization technologies. In fact, some investigators in the past have used photolithography [4] to achieve a selective emitter or texturization, defeating the purpose of reducing cost by screen printing. In contrast to CFP, which generally involves multiple furnace diffusions and oxidations at high temperatures, extensive wafer cleaning, and use of more chemicals and gases, RTP significantly reduces the cell fabrication time, thermal budget [5], and wafer cleaning steps. Use of SP contacts greatly simplifies contact formation compared with photolithography (PL) which requires spin-on, bake, exposure, and development of photoresist followed by evaporation, lift-off, and plating of metal. Finally, PECVD of SiN provides antireflection (AR) properties and surface and bulk defect passivation. In addition, PECVD is a low-temperature process and can be done in a batch reactor [6]. In fact, ASE Americas, Inc. (formerly Mobil Solar Energy Corp.) [7] and R&S Renewable Energy Systems B.V. [3] have been successful in implementing PECVD in an industrial setting suggesting the cost-effectiveness of the technology.

It is important to note that before RTP can be considered a viable alternative to CFP for photovoltaic devices, RTP systems must evolve from single-wafer to batch-mode processing. In fact, one such machine which has recently become available can process multiple wafers uniformly over an area of 35 cm $\times$ 35 cm or 12 100-cm^2 cells at a time [8]. Since an emitter and back surface field (BSF) can be formed by RTP in a matter of seconds or minutes, high throughputs are already possible with *existing* equipment. Even greater throughputs are conceivable if, for example, simple modifications such as retrofitting RTP lamps into a continuous belt-line system are realized. In contrast, typical CFP diffusion times are at least 30 min. Therefore, throughputs for emitter diffusion alone are typically limited to only 150–250 wafers/h per furnace tube and 400–500 wafers/h per IR belt furnace. BSF formation would require an additional lengthy step. Thus, current means of diffusion generally bottleneck the production line, and RTP may provide the solution with shorter processing times and greater cell efficiencies.

In previous publications, we demonstrated high-efficiency RTP cells of 17.1%, 16.8%, 14.8%, and 15.1% on FZ, Cz, multicrystalline, and dendritic web silicon, respectively [9], [10]. These cells were processed by rapid, simultaneous front

Manuscript received October 2, 1996. The review of this paper was arranged by Editor P. N. Panayotatos. This work was supported by Sandia National Laboratories under Contract A0-6162 and by the National Institute of Standards under Contract 70NANB5H1071-GIT.

The authors are with the University Center of Excellence for Photovoltaics Research and Education, Department of Electrical and Computer Engineering, Georgia Institute of Technology, Atlanta, GA 30332 USA.

Publisher Item Identifier S 0018-9383(97)06124-8.

0018–9383/97$10.00 © 1997 IEEE

Authorized licensed use limited to: Sidley Austin LLP. Downloaded on June 22,2024 at 19:31:14 UTC from IEEE Xplore. Restrictions apply.

and back diffusion of the emitter and BSF without any high-temperature furnace steps; however, photolithography was used to define the front evaporated contacts (hereafter referred to as the RTP/PL process). Since most solar cell manufacturers do not regard photolithography as a cost-effective technique for contact formation for terrestrial photovoltaics, we modified the RTP process to accommodate screen-printed contacts. Since the emitters of these RTP/PL cells were too shallow (~ 0.14 μm) for screen printing, the RTP diffusion had to be adjusted for greater junction depths. Thus, development of the RTP/SP process required formulating both the diffusion and contact firing cycles.

In a recent study, we demonstrated cell efficiencies in the 14%–15% range made by the RTP/SP process [11]. The efficiency of these cells were limited to this range because of the heavy doping recombination in the 20–30 Ω/sq. emitter and front surface recombination. Recent improvements [12] have resulted in $>1\%$ increase in cell efficiency by lowering the concentration of the phosphorus spin-on source to increase the emitter sheet resistance (ρ_s) and by providing front surface passivation with PECVD SiN. In this study, we first examine the importance of the emitter design for RTP/SP cell performance followed by detailed modeling and characterization used to quantify the efficiency limiting mechanisms of these 16%-efficient RTP/SP/PECVD cells.

II. Device Fabrication

RTP/SP/PECVD n^+-p-p^+ cell fabrication in this study involved simultaneous formation of an emitter and BSF using phosphorus spin-on dopants on the front and 1 μm aluminum evaporated on the back. Two concentrations of phosphorus spin-on dopants were used: 10^{21} and 10^{20} cm^{-3}. The RTP diffusion temperature/time was varied for the desired ρ_s. Prior to printing contacts, SiN was deposited by PECVD. Deposition conditions involved an RF power of 30 W operating at 13.6 MHz, pressure of 0.9 torr, and deposition temperature of 300 °C.

The front grid contact was formed by screen printing commercially available silver pastes on top of the SiN and then "fired through" the film. Firing screen-printed contacts proved to be extremely critical in order to prevent shunting of these shallow ($x_j < 0.3$ μm) RTP junctions while obtaining minimum contact resistance. After numerous experiments, an RTP firing cycle of 737 °C for only 10 s in high-purity air was established. In some cases, a 715 °C/90 s contact firing cycle was developed for furnace use instead of the RTP system. The contact quality was virtually independent of which contact firing system used. In this work, the back contact was formed by evaporation of Al/Ti/Pd/Ag followed by a 400 °C/10 min contact anneal in forming gas. Work is in progress to replace both the Al BSF and back contact evaporations by a single Al BSF screen printing step. This would significantly simplify the process, while at the same time, improve the long wavelength response because of a deeper BSF profile and lower back surface recombination velocity (BSRV) [13]. The final step was an evaporation of MgF_2 as a second layer AR coating; however, it is important to note that this was used because cells would be tested in air $(n = 1.0)$. In practice, this second layer would not be deposited for cells in a module, which are under glass $(n = 1.5)$.

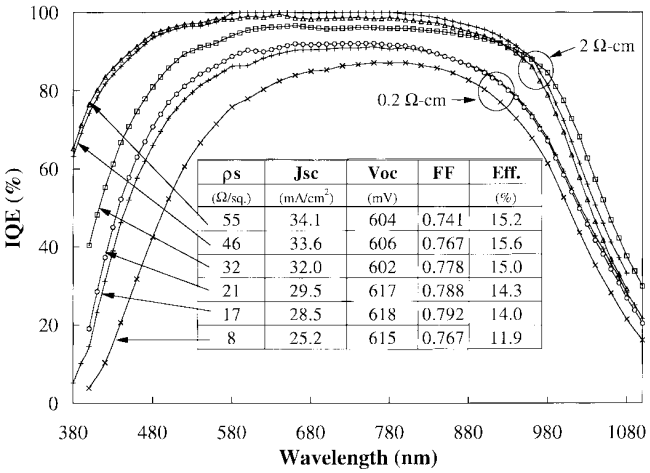

Fig. 1. Optimization of RTP/SP emitter sheet resistance (ρ_s).

Preparation of CFP/PL cells was as follows. After an initial wafer clean, phosphorus diffusion was carried out at 930 °C for 30 min in addition to a ramp-up and ramp-down rate of 5 °C/min from 500 °C. This yields a sheet resistance of about 15 Ω/sq. which is then slowly etched back to about 120 Ω/sq. After a second cleaning, 1 μm of Al was evaporated on the back side followed by a 850 °C/30 min drive-in to form the back surface field (BSF). During this step, a 10-nm oxide was also grown on the front and a 30 min forming gas anneal was performed after ramping down to 400 °C at 5 °C/min After evaporation of the back Al/Ti/Pd/Ag contact, a series of photolithography steps were done to define the front grid contact. Finally individual cells were isolated through a mesa etch followed by evaporation of a ZnS/MgF_2 double layer AR coating optimized for silicon in air.

III. Results and Discussions

A. Optimization of RTP/SP Emitter Sheet Resistance

Design of the emitter region is extremely important for achieving high-efficiency RTP/SP cells. A low surface concentration improves front surface passivation but increases contact resistance. A shallow junction depth improves short wavelength collection efficiency but increases the susceptibility of shunting. Given these trade-offs, experiments were performed to optimize the ρ_s of the homogeneous RTP/SP emitter. Fig. 1 shows the results of RTP/SP cells as a function of ρ_s in the range of 8–55 Ω/sq. Instead of SiN, these cells had ZnS/MgF_2 AR coatings to prevent short wavelength absorption from perturbing internal quantum efficiency (IQE) measurements. All cells were RTP diffused at 930 °C (±15 °C) using the 10^{21} cm^{-3} spin-on source except for the two higher ρ_s values of 46 and 55 Ω/sq. which were formed using the 10^{20} cm^{-3} spin-on source. As expected, substantial improvements in the short wavelength response and J_{sc} occurs with increasing ρ_s. However, there is a trade-off because of the degradation of

Authorized licensed use limited to: Sidley Austin LLP. Downloaded on June 22,2024 at 19:31:14 UTC from IEEE Xplore. Restrictions apply.

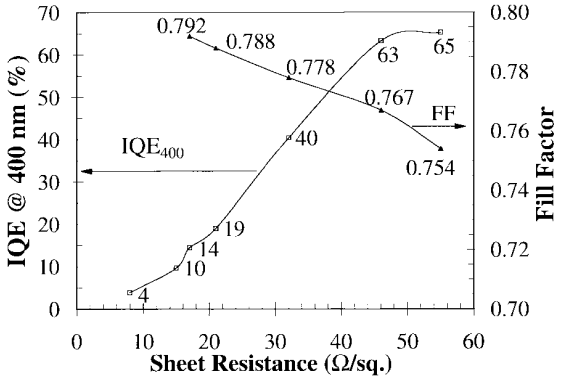

Fig. 2. Competition between enhanced short wavelength response and degraded FF with increasing ρ_s.

fill factor (FF) with increasing ρ_s (Fig. 2). FF decreases with higher ρ_s because of increased contact resistance and ohmic losses in the emitter sheet. Fig. 2 depicts a fairly linear ρ_s dependence for both the increasing IQE response at 400 nm and decreasing FF. Considering this competition in terms of cell efficiency, the optimum ρ_s for the homogeneous RTP/SP emitter was found to be in the 40–50 Ω/sq. range. Of course, the ideal emitter for screen-printed contacts is a selective emitter in which a very high ρ_s ($\geq$100 Ω/sq.) is tailored in the field region (between grid fingers) to achieve higher short wavelength response, while a very low ρ_s ($\leq$15 Ω/sq.) remains underneath the contacts to limit contact resistance losses and prevent shunting.

B. RTP/SP/PECVD Cells on 4 cm^2 Cz and 25 cm^2 FZ Silicon

Based on the optimization of emitter sheet resistance, many RTP/SP/PECVD runs were performed. Table I shows several of the many $\geq$16%-efficient 4 cm^2 FZ cells that were fabricated by the RTP/SP/PECVD process—demonstrating the reproducibility of the process. The same process on 4 cm^2 Cz silicon cells gave an efficiency of 15.9%. Preliminary work on larger area 25 cm^2 cells have resulted in 15.4% efficient FZ cells. These efficiencies are quite attractive for commercial cells. In addition the front and back diffusion times are much shorter than commercial cells.

IV. Device Modeling and Characterization (RTP/SP/PECVD versus CFP/PL)

To improve efficiencies further, it is important to identify what limits current RTP/SP/PECVD cells to about 16%. Based on a comparison between our high-throughput RTP/SP/PECVD process and the standard CFP/PL process used in the laboratory, we will identify all of the efficiency limiting mechanisms in the RTP/SP/PECVD approach through a detailed modeling and characterization study. Fig. 3 shows that compared with an optimized CFP/PL cell, the RTP/SP/PECVD cell gives ~2% lower cell efficiency because of a decrease in J_{sc} and FF. In this experiment, $\Delta J_{sc} = 2.5$ mA/cm^2 and $\Delta FF = 0.024$. We will show that this 2% efficiency gap can be explained on the basis of four categories:

TABLE I
High-Efficiency RTP/SP/PECVD Cells

Run # (Cell ID)	V_{oc} (mV)	J_{sc} (mA/cm^2)	FF	Eff (%)
4 cm^2 float-zone silicon (2 Ω-cm)				
6fz2-4	612	34.0	0.770	16.0[a]
8fz3-4	616	34.4	0.761	16.1[a]
10fz4-4	612	34.0	0.785	16.3[a]
10fz5-4	612	34.1	0.774	16.2[a]
13fz2-1	610	34.3	0.767	16.0
14fz4-4	615	34.2	0.764	16.1
10fz2-4	629	32.3	0.765	15.6[b]
4 cm^2 Czochralski silicon (3 Ω-cm)				
10fz1-1	605	33.9	0.774	15.9[a]
12fz5-1	599	33.5	0.760	15.2
cz9-4	592	32.2	0.779	14.8[a]
25 cm^2 float-zone silicon (0.2 Ω-cm)				
7fz2	633	31.4	0.773	15.4[a,b]

[a] Tested and verified by Sandia National Laboratories.
[b] Base resistivity = 0.2 Ω-cm.

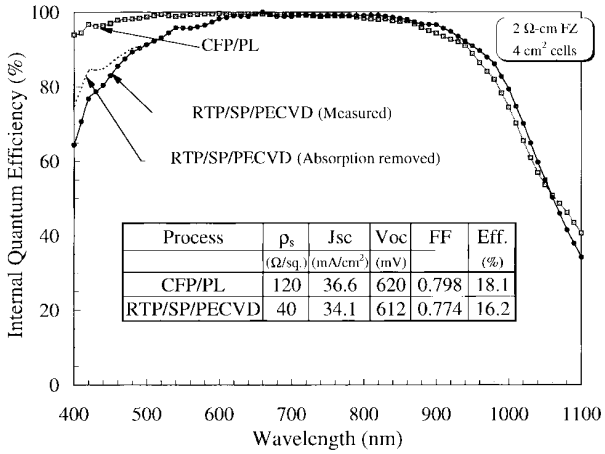

Fig. 3. Comparison of CFP/PL and RTP/SP/PECVD cells.

short wavelength response, reflectance, quality of (grid) contacts, and long wavelength response.

A. Short Wavelength Losses of the RTP/SP/PECVD Cell Resulting from SiN Absorption and Emitter Recombination

Comparing the IQE of the two cells in Fig. 3 reveals that most of the difference between the RTP/SP/PECVD and CFP/PL cells lies in the short wavelength response. To compute the amount of short circuit current density lost in the short wavelength, the IQE (between 400 and 800 nm) of the two cells were multiplied with the photocurrent density of the AM1.5 global solar spectrum (q^*N_{ph}, where q is the unit of electronic charge and N_{ph} is the photon flux)

$$\Delta J_{sc}|_{short_\lambda} = q \sum_{\lambda=400\ nm}^{800\ nm} [N_{ph}(\lambda)|_{AM1.5G} \cdot IQE_1(\lambda)] - q \sum_{\lambda=400\ nm}^{800\ nm} [N_{ph}(\lambda)|_{AM1.5G} \cdot IQE_2(\lambda)], \quad (1)$$

Authorized licensed use limited to: Sidley Austin LLP. Downloaded on June 22,2024 at 19:31:14 UTC from IEEE Xplore. Restrictions apply.

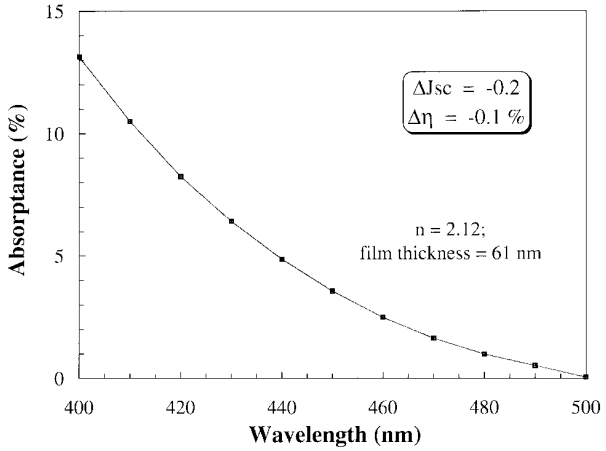

Fig. 4. Calculated parasitic absorption in the SiN antireflection coating used in the RTP/SP/PECVD cell.

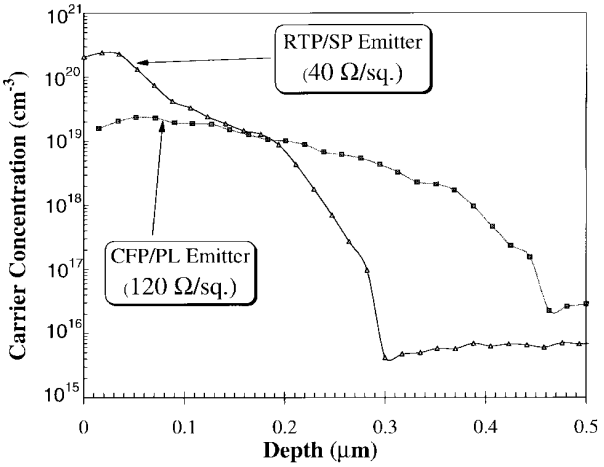

Fig. 5. Comparison of emitter profiles. Profiles measured by spreading resistance analysis.

This gave a difference of 1.1 mA/cm^2. (Note that (1) is unaffected by reflectance since the summation is taken over the IQE. Reflectance loss is considered separately in the next section.) Three mechanisms explain this short wavelength loss: 1) parasitic absorption in SiN; 2) front surface recombination; and 3) heavy doping recombination in the emitter. To characterize the absorption component, spectroscopic ellipsometry measurements were performed to measure the extinction coefficient as a function of wavelength. This data was then used in the CAMS AR coating software to compute the absorptance, $A(\lambda)$, as a function of wavelength. Fig. 4 shows the computed absorptance for a SiN film which had a refractive index (n) of 2.12 at 632.8 nm. To calculate the absorption-induced $J_{\rm sc}$ loss, the absorptance from Fig. 4 was multiplied with the photocurrent ($q^*N_{\rm ph}$) of the AM1.5G spectrum and IQE (at each wavelength),

$$J_{\rm sc}|_{\rm Absorb} = q\sum_{\lambda} N_{\rm ph}(\lambda)|_{\rm AM1.5G} A(\lambda){\rm IQE}(\lambda). \qquad (2)$$

The loss in $J_{\rm sc}$ attributed to SiN absorption was found to be only 0.2 mA/cm^2 for the $n = 2.12$ film..

The remaining 0.9 mA/cm^2 of the observed 1.1 mA/cm^2 loss in the short wavelength must come from front surface recombination and heavy doping effects such as Auger recombination and bandgap narrowing in the emitter. To verify this, emitters were first characterized by spreading resistance analysis (SRA), and then the influence of the emitter profiles on device performance was modeled by the PC-1D semiconductor device simulator [14]. The measured profiles in Fig. 5 show that the 40 Ω/sq. RTP/SP emitter compared with the 120 Ω/sq. CFP/PL emitter has an order of magnitude greater surface electron concentration. The combination of higher surface concentration and difference in surface passivation (oxide for the CFP/PL cell and SiN for the RTP/SP/PECVD cell) gives rise to more severe heavy doping effects and a greater front surface recombination velocity (FSRV) for the RTP/SP emitter. PC-1D was effective in decoupling these two loss mechanisms. To extract the FSRV, the measured IQE was matched with the PC-1D-calculated IQE (Fig. 6). For the RTP/SP/PECVD cell, the IQE was

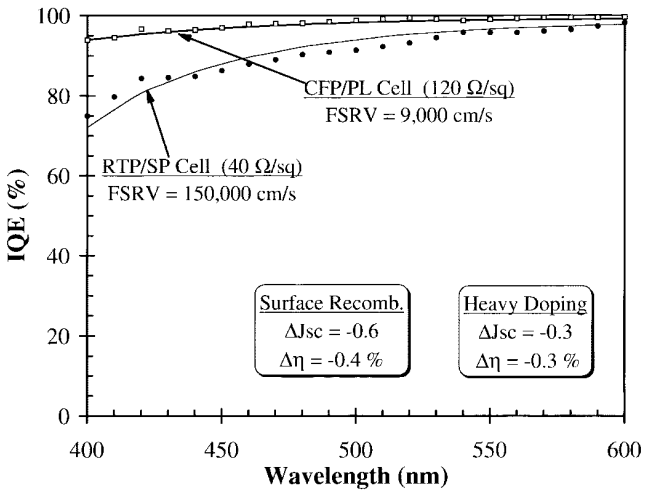

Fig. 6. PC-1D simulations to fit short wavelength response and calculate emitter surface recombination and heavy doping losses.

first corrected by removing the effect of SiN absorption (as shown in Fig. 3) using the data in Fig. 4. Fig. 6 shows that the FSRV was found to be about 9000 (±1000) cm/s for the CFP/PL emitter and about 150 000 (±25 000) cm/s for the RTP/SP emitter. This translates into a loss of 0.6 mA/cm^2 in $J_{\rm sc}$ and 4 mV in $V_{\rm oc}$ (determined by reducing the FSRV value from 150 000 to 9000 in the PC-1D simulation of the RTP/SP cell). Finally, giving the RTP/SP cell the CFP/PL emitter profile (i.e., increasing the ρ_s from 40 Ω/sq. to 120 Ω/sq.) gave an additional increase of 0.3 mA/cm^2 in $J_{\rm sc}$ and 4 mV in $V_{\rm oc}$ because of the reduction in heavy doping effects. Thus, absorption (0.2 mA/cm^2), surface passivation (0.6 mA/cm^2), and heavy doping effects (0.3 mA/cm^2) account for the 1.1 mA/cm^2 gap in short wavelength IQE between the RTP/SP/PECVD and CFP/PL cells. In addition, SRA characterization in conjunction with PC-1D modeling was in very good agreement with cell performance and IQE data.

The question of what steps can be taken to reduce this gap in the short wavelength IQE arises. Our first attempt

Authorized licensed use limited to: Sidley Austin LLP. Downloaded on June 22,2024 at 19:31:14 UTC from IEEE Xplore. Restrictions apply.

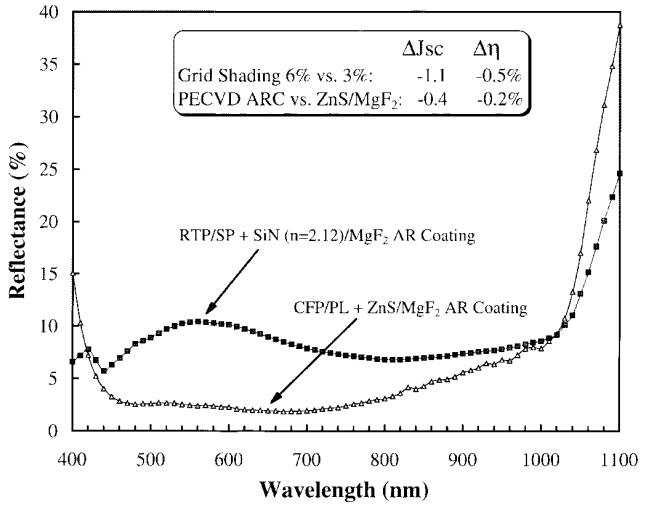

Fig. 7. Reflectance comparison between RTP/SP and CFP/PL cells.

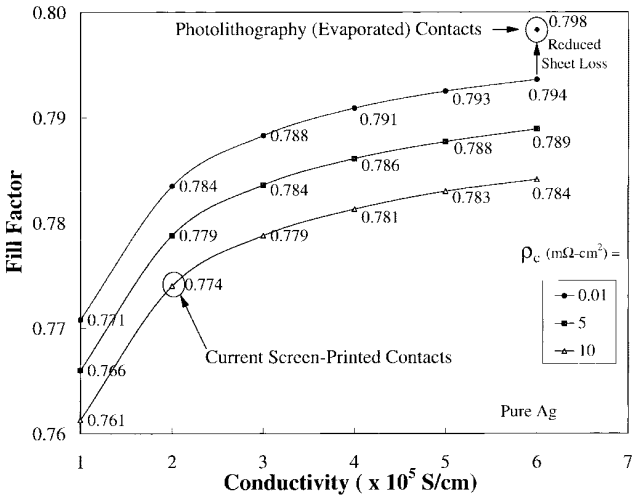

Fig. 8. Grid simulations used to compare SP and PL contacts.

was to fabricate RTP/PL cells with a conventional furnace oxide (CFO). This resulted in cells as high as 17.9% in efficiency (confirmed by Sandia National Laboratories) with a J_{sc} of 35.9 mA/cm^2, V_{oc} of 618 mV, and FF of 0.805—nearly closing the gap with the 18.1% CFP/PL cell (in Fig. 3) fabricated on the same material. Such a process, however, required a lengthy furnace process (to grow a passivating oxide) which reduces the attractiveness of RTP. A higher throughput alternative is to provide rapid thermal oxide (RTO) passivation. Recent success, by others [15], with an RTO to enhance the short wavelength response of RTP/PL cells has been encouraging. We have also been successful in RTO passivation of RTP/PL cells and have observed improvements of about 1% (absolute) in cell efficiency when compared with unpassivated cells [16]. This has resulting in $\geq$18%-efficient RTP cells (with photolithographically-defined contacts) on Cz and FZ silicon [16]. Attempts are underway to screen print RTO passivated cells.

B. Reflectance Losses Resulting from Screen-Printed Grid Shading and AR Coatings

The second major component of the efficiency difference between RTP/SP/PECVD and CFP/PL cells was found to be the difference in reflectance. Fig. 7 shows that the reflectance of the RTP/SP/PECVD cell is considerably greater than that of CFP/PL cell. Multiplying these reflectances with the spectrum and IQE,

$$\Delta J_{sc}|_{\text{Refl}} = q\sum_{\lambda} N_{\text{ph}}(\lambda)|_{\text{AM1.5G}} \times [R_2(\lambda)\text{IQE}_2(\lambda) - R_1(\lambda)\text{IQE}_1(\lambda)] \quad (3)$$

reveals that about 1.5 mA/cm^2 is lost because of the difference in reflectance. Most of the current loss is due to the difference in grid shading factor, which in this case is about 6% for SP cells and 3% for PL cells. Currently, our SP grid contains finger widths of 125 μm compared with only about 25 μm for the PL grid. Grid shading in the SP cell therefore accounts for about 1.1 mA/cm^2 (3% of 36.6) of the J_{sc} difference indicating that substantial improvement can be realized if fine-line ($\leq$60 μm) printing, demonstrated by others [1]–[4], can be implemented at low cost. The remaining 0.4 mA/cm^2 is due to the difference between SiN-based $(n = 2.12)$ and ZnS-based $(n = 2.36)$ AR coatings. This difference would be eliminated if a SiN refractive index of 2.3–2.4 is used, however, a penalty in terms of increased SiN-absorption would ensue. The lower index was used because recent work [17] has indicated that the emitter saturation current density (and therefore FSRV) is minimized at a SiN index of 2.1. Work is in progress to optimize PECVD AR coatings to deliver the best combination of minimum reflectance, low absorption, and optimum surface passivation.

C. Ohmic Losses Related to the Quality of Screen-Printed Contacts

The screen-printed cell in Fig. 3 gives about 0.024 lower FF, which can be attributed to the inferior quality of SP contacts compared with evaporated PL contacts. Nevertheless, SP is justified on economic grounds by most photovoltaic manufacturers. To determine what components explain the FF loss so that it can be minimized, we first characterized the specific contact resistance (ρ_c) and conductivity (σ) of the SP contacts and then used these parameters in our grid modeling software to analyze the ohmic losses throughout the grid and emitter sheet. To measure the contact parameters, contact resistance and conductivity measurement structures were fabricated in accordance with the TLM method [18]. These values were found to be about $\sigma = 2 \times 10^5$ S/cm and $\rho_c = 10$ mΩ-cm^2 and then used as inputs for the grid model calculations (Fig. 8) to evaluate our (eight-finger) SP grid design. Calculations revealed that about 0.01 is lost in FF because of the factor of three lower conductivity of SP contacts compared with pure silver PL contacts, and another 0.01 is lost because of the contact resistance (which is negligible for PL contacts). There is an additional component resulting from the ohmic power loss in the emitter sheet. This term can be

Authorized licensed use limited to: Sidley Austin LLP. Downloaded on June 22,2024 at 19:31:14 UTC from IEEE Xplore. Restrictions apply.

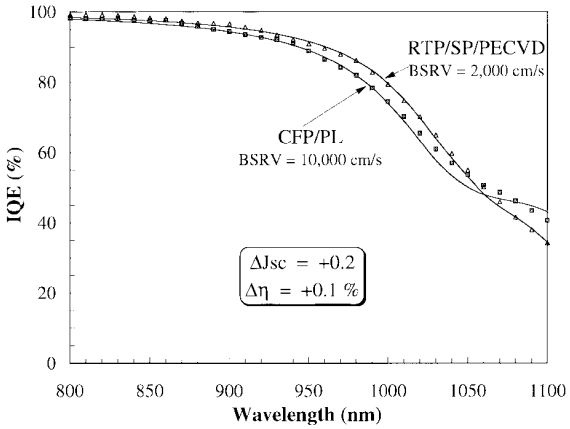

Fig. 9. PC-1D simulations to fit long wavelength response and estimate back surface recombination velocity (BSRV).

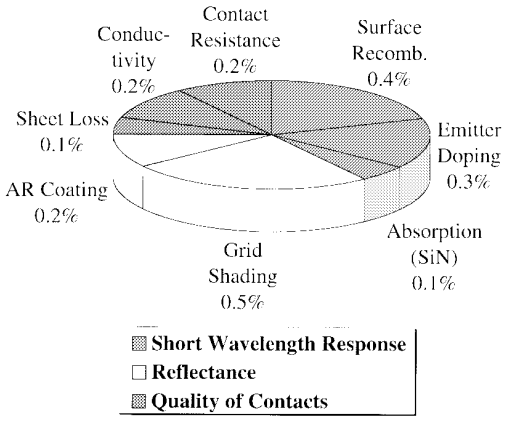

Fig. 10. Components of the 2% efficiency difference between RTP/SP/PECVD and CFP/PL cells.

calculated by [19]

$$P_{\text{sheet}} = \frac{1}{12}(J_{mp})^2(\rho_s)S^2 \cdot 1000 \tag{4}$$

where P_{sheet} is the power loss in mW/cm^2 and S is the spacing (in centimeters) between fingers. Although the 40 Ω/sq. RTP/SP emitter has a factor of three lower ρ_s, there is a factor of 2.5 greater spacing for the SP grid, making P_{sheet} dominate in favor of the PL grid. Thus, the combination of contact resistance, conductivity, and emitter sheet loss explains the observed loss in FF.

D. Improved Long Wavelength Response of the RTP/SP/PECVD Cell Resulting from Reduced Back Surface Recombination

Although most of the difference between the two cells lies in the short wavelengths, there is an additional small difference between the two cells in the long wavelength response (Fig. 3). Multiplying this difference with the solar spectrum and IQE (as in (1), but over the wavelength range of 800–1100 nm) reveals that the RTP/SP/PECVD cell gives 0.2 mA/cm^2 greater current density in the long wavelength. To decouple whether the difference is due to bulk lifetime

TABLE II
SUMMARY OF LOSS MECHANISMS FOR THE RTP/SP/PECVD PROCESS COMPARED WITH THE CFP/PL PROCESS

Source of Loss	CFP/PL	RTP/SP	ΔJ_{sc} or ΔFF (mA/cm^2)	ΔEff (%)
1. Short Wavelength Response				
FSRV (cm/s)	9,000	150,000	-0.6	0.4
Emitter Doping	120 Ω/sq.	40 Ω/sq.	-0.3	-0.3
SiN Absorption	NA	k ≠ 0	-0.2	-0.1
2. Reflectance				
Grid Shading	3%	6%	-1.1	-0.5
AR Coating	ZnS/MgF_2	SiN/MgF_2	-0.4	-0.2
3. Quality of Contacts				
Contact Res.	Negligible	10 mΩ-cm^2	-0.01	-0.2
Conductivity (S/cm)	$6x10^5$	$2x10^5$	-0.01	-0.2
Finger Spacing	1.0 mm	2.5 mm	-0.004	-0.1
4. Long Wavelength Response				
BSRV (cm/s)	10,000	2,000	+0.2	+0.1
Total Calculated Losses:			ΔJ_{sc}=2.4 ΔFF=0.024	Δη=1.9%
Actual Losses:			ΔJ_{sc}=2.5 ΔFF=0.024	Δη=1.9%

(τ_b) or back surface recombination, the τ_b of both cells was measured by the PCD technique [20] on cells etched down to bare silicon and immersed in HF to passivate the surface. It was found that τ_b was 275 μs for the CFP/PL cell and 350 μs for the RTP/SP/PECVD cell. Since for both cases, the bulk diffusion length to cell thickness ratio is high, both cells are surface dominated. To estimate the effective back surface recombination velocity (BSRV) at the p-p$^+$ interface, PC-1D was used to match the calculated long wavelength IQE to the measured data (Fig. 9). The BSRV was estimated to be about five times lower for the RTP/SP/PECVD cell (BSRV $\cong$ 2000 cm/s) compared with the CFP/PL cell (BSRV $\cong$ 10 000 cm/s). The difference in BSRV is attributed to the difference in aluminum BSF profiles which were formed at different alloy temperatures. Since the BSF alloy temperature for the RTP/SP/PECVD cell was 930 °C compared with 850 °C for the CFP/PL cell, the higher temperature BSF will have a greater junction depth (in accordance with the Al/Si phase diagram [21]), thus reducing the BSRV. Others have also shown substantial improvement with increased aluminum BSF alloy temperatures by both CFP [22], [23] and RTP [23] technologies. Table II summarizes all of the efficiency loss mechanisms of the RTP/SP/PECVD process.

V. CONCLUSION

In summary, we present the first successful integration of three rapid, low-cost, high-throughput technologies with manufacturable cell efficiencies in the range of 15%–16% on single-crystal silicon. We have shown that emitter design is critical for these cells. A ρ_s of 40–50 Ω/sq. was determined as the optimum, given the trade-off between short wavelength response and fill factor. Detailed modeling and characterization of these novel cells was presented to decouple all of the RTP/SP/PECVD efficiency-limiting mechanisms (Fig. 10) and to provide fundamental understanding and guidelines for further improvements. On the basis of this in-depth analysis,

Authorized licensed use limited to: Sidley Austin LLP. Downloaded on June 22,2024 at 19:31:14 UTC from IEEE Xplore. Restrictions apply.

the performance of these RTP/SP/PECVD cells can be raised intelligently and systematically to reduce the efficiency gap between these and CFP/PL cells. In an upcoming publication [16], we demonstrate that the gap between RTP/PL and CFP/PL cell efficiencies is eliminated by applying high quality rapid thermal oxide (RTO) passivation; thus, the difference in performance is related to screen printing losses and not RTP. Research is in progress to implement rapid thermal oxidation for surface passivation, low-cost selective emitters to reduce emitter recombination while preserving fill factor, and deeper aluminum BSF's by screen-printed aluminum to reduce back surface recombination. The success of the RTP/SP/PECVD process suggests that use of these promising technologies in industry would result in significant cost reduction and high-efficiency cells.

ACKNOWLEDGMENT

The authors would like to thank Dr. G. E. Jellison, Jr., of Oak Ridge National Laboratories for spectroscopic ellipsometry measurements and Dr. D. Ruby and coworkers at Sandia National Laboratories for cell testing and verification.

REFERENCES

[1] J. Nijs, E. Demesmaeker, J. Szlufcik, J. Poortmans, L. Frisson, K. De Clercq, M. Ghannam, R. Merterns, and R. Van Overstraeten, "Latest efficiency results with the screenprinting technology and comparison with the buried contact structure," in *Proc. 24th IEEE Photovoltaic Specialists Conf.*, Piscataway, NJ, 1994, pp. 1242–1249.

[2] H. Nakaya, M. Nishida, Y. Takeda, S. Moriuchi, T. Tonegawa, T. Machida, and T. Nunoi, "Polycrystalline silicon solar cells with V-grooved surface," in *Tech. Dig. Int. Photovoltaic Solar Energy Conf.*, Nagoya, Japan, 1993, pp. 91–92.

[3] L. Verhoef, P.-P. Michiels, R. J. C. van Zolingen, H. H. C. de Moor, A. Burgers, R. Steeman, and W. Sinke, "Low-cost multicrystalline silicon solar modules with 16% encapsulated cell efficiency," in *Proc. 24th IEEE Photovoltaic Specialists Conf.*, Piscataway, NJ, 1994, pp. 1547–1550.

[4] K. Fukui, H. Yamashita, M. Takayama, K. Okada, K. Masuri, K. Shirasawa, and H. Watanabe, "15 cm $\times$ 15 cm high efficiency multicrystalline silicon solar cell," in *Proc. 22nd IEEE Photovoltaic Specialists Conf.*, Piscataway, NJ, 1991, pp. 1040–1044.

[5] R. P. S. Thakur *et al.*, "Thermal budget considerations in rapid isothermal processing," *Appl. Phys. Lett.*, vol. 64, pp. 327–329, 1994.

[6] C. Leguijt, P. Lölgen, J. A. Eikelboom, A. W. Weeber, F. M. Schuurmans, W. C. Sinke, P. F. A. Alkemade, P. M. Sarro, C. H. M. Marée, and L. A. Verhoef, "Low temperature surface passivation for silicon solar cells," *Sol. Energy Materials Sol. Cells*, vol. 40, pp. 297–345, Aug. 1996.

[7] R. Gonsiorawski and G. Czernienko, "Method of fabricating solar cells with silicon nitride coating," U. S. Patent 4 751 191, assigned to Mobil Solar Energy Corporation, issued June 14, 1988.

[8] Product information regarding "RTP solar cell furnace," Vortek Industries, Vancouver, B.C., Canada.

[9] P. Doshi, A. Rohatgi, M. Ropp, Z. Chen, D. Ruby, and D. L. Meier, "Rapid thermal processing of high-efficiency silicon solar cells with controlled *in-situ* annealing," *24th IEEE Photovoltaic Specialists Conf.*, 1994, pp. 1299–1302.

[10] A. Rohatgi, P. Doshi, M. Ropp, L. Cai, W. A. Doolittle, S. Narasimha, T. Krygowski, J. Rand, D. Ruby, and D. L. Meier, "Improved understanding and optimization of RTP and PECVD processes for high-efficiency silicon solar cells," *13th Europ. Photovoltaic Solar Energy Conf.*, Nice, France, Oct. 23–27, 1995.

[11] P. Doshi, J. Mejia, K. Tate, and A. Rohatgi, "Integration of screen-printing and RTP technologies for silicon solar cell fabrication," *IEEE Electron Device Lett.*, vol. 17, pp. 404–406, Aug. 1996.

[12] P. Doshi, J. Mejia, K. Tate, S. Kamra, A. Rohatgi, S. Narayanan, and R. Singh, "High-efficiency silicon solar cells by low-cost rapid thermal processing, screen-printing, and plasma enhanced chemical vapor deposition," in *Proc. 25th IEEE Photovoltaic Specialists Conf.*, Piscataway, NJ, 1996.

[13] S. Narasimha, J. Mejia, and A. Rohatgi, "Screen-printed aluminum back surface fields for silicon solar cells," in *6th Workshop Role Impurities Defects Silicon Device Processing*, Snowmass, CO, Aug. 12–14, 1996.

[14] P. Basore, "PC-1D version 3: Improved speed and convergence," in *Proc. 22nd IEEE Photovoltaic Specialists Conf.*, Piscataway, NJ, 1991, pp. 299–302.

[15] S. Sivoththaman, W. Laureys, P. Schepper, J. Nijs, and R. Mertens, "Rapid thermal processing of conventionally and electro-magnetically cast 100 cm^2 multicrystalline silicon," in *Proc. 25th IEEE Photovoltaic Specialists Conf.*, Piscataway, NJ, 1996.

[16] P. Doshi and A. Rohatgi, "18% efficient silicon photovoltaic devices by rapid thermal diffusion and oxidation," *IEEE Trans. Electron Devices*, submitted for publication.

[17] L. Cai, "Improved understanding and control of the properties of SiN films and its applications to silicon solar cells," Ph.D. dissertation, Georgia Inst. Technol., Atlanta, 1997.

[18] D. K. Schroder, "Contact resistance and schottky barrier height," in *Semiconductor Material and Device Characterization*. New York: Wiley, 1990, pp. 114–121.

[19] N. Wyeth, "Sheet resistance component of the series resistance in a solar cell as a function of grid geometry," *Solid State Electron.*, vol. 20, pp. 629–634, 1977.

[20] D. E. Kane and R. M. Swanson, "Measurement of the emitter saturation current by a contactless photoconductivity decay method," in *Proc. 18th IEEE Photovoltaic Specialists Conf.*, Piscataway, NJ, 1985, pp. 578–583.

[21] P. Lölgen, "Surface and volume recombination in silicon solar cells," Ph.D. dissertation, Utrecht Univ., The Netherlands, pp. 58–59, 1995.

[22] S. Naryanan and M. Green, "Improvement in the open-circuit voltage and efficiency of silicon solar cells by rear aluminum treatment," *Sol. Cells*, vol. 26, pp. 329–334, 1989.

[23] P. Hahne, W. Wettling, and R. Schindler, "Aluminum back surface field doping profiles by conventional and rapid thermal processing," in *12th Europ. Photovoltaic Solar Energy Conf.*, Amsterdam, The Netherlands, 1994.

Parag Doshi received the B.S. degree in electrical engineering from the Georgia Institute of Technology, Atlanta, in 1992. He is currently pursuing the Ph.D. degree in electrical engineering at the Georgia Institute of Technology.

He is a Member of the University Center of Excellence for Photovoltaics Research and Education, Georgia Institute of Technology. His research interests include the design, modeling, fabrication, and characterization of high-efficiency silicon solar cells. His Ph.D. dissertation concerns rapid thermal processing, PECVD of SiN and SiO_2 films, and screen printing technologies for cost-effective fabrication of high-efficiency photovoltaic devices.

Jose Mejia received the B.S. degree in electrical engineering from the Georgia Institute of Technology, Atlanta, in 1994.

He is currently a Research Engineer with the University Center of Excellence for Photovoltaics Research and Education in the School of Electrical and Computer Engineering, Georgia Institute of Technology. His work includes the fabrication and characterization of high-efficiency silicon solar cells. His research interests include rapid thermal processing and screen printing technologies for cost-effective fabrication of high-efficiency photovoltaic devices.

Authorized licensed use limited to: Sidley Austin LLP. Downloaded on June 22,2024 at 19:31:14 UTC from IEEE Xplore. Restrictions apply.

Keith Tate is with ITT Night Vision, Roanoke, VA where he is developing the fourth generation of photocathodes for night vision devices. Before joining ITT, he was a Research Equipment Specialist at the University Center of Excellence for Photovoltaics Research and Education in the School of Electrical and Computer Engineering, Georgia Institute of Technology, Atlanta. He was with Georgia Institute of Technology between 1977 and 1988 working in the area of high-efficiency silicon photovoltaic devices.

Ajeet Rohatgi (M'78–SM'86–F'91) received the B.S. degree in electrical engineering from the Indian Institute of Technology, Kanpur, in 1971, the M.S. degree in materials engineering from the Virginia Polytechnic Institute and State University, Blacksburg, in 1973, and the Ph.D. degree in metallurgy and material science from Lehigh University, Bethlehem, PA, in 1977.

Before joining the Electrical Engineering Faculty at Georgia Institute of Technology, Atlanta, in 1985, he was a Westinghouse Fellow at the Research and Development Center, Pittsburgh, PA. He is a Georgia Power Distinguished Professor in the School of Electrical Engineering and the director of the University Center of Excellence for Photovoltaic Research and Education, Georgia Institute of Technology. His current research interests include modeling and fabrication of high-efficiency silicon and compound semiconductor solar cells; silicon MOS devices; semiconductor material and device characterization; defects and recombination in semiconductors; and MBE and MOCVD growth of compound semiconductors for optoelectronic and photovoltaic devices.

Dr. Rohatgi received the Westinghouse Engineering Achievement Award for the "Design and Fabrication of High Efficiency Silicon Solar Cells."

Authorized licensed use limited to: Sidley Austin LLP. Downloaded on June 22,2024 at 19:31:14 UTC from IEEE Xplore. Restrictions apply.